NANO LETTERS

Letter

pubs.acs.org/NanoLett

Aerobic Oxidation of Cyclohexane on Catalysts Based on Twinned and Single-Crystal $Au_{75}Pd_{25}$ Bimetallic Nanocrystals

Liangbing Wang,[†] Songtao Zhao,[†] Chenxuan Liu, Chen Li, Xu Li, Hongliang Li, Youcheng Wang, Chao Ma, Zhenyu Li,* and Jie Zeng*

Hefei National Laboratory for Physical Sciences at the Microscale, Key Laboratory of Strongly-Coupled Quantum Matter Physics of Chinese Academy of Sciences, Center of Advanced Nanocatalysis (CAN-USTC), CAS Centre for Excellence and Synergetic Innovation Centre in Quantum Information and Quantum Physics, Department of Chemical Physics, University of Science and Technology of China, Hefei, Anhui 230026, P. R. China

Supporting Information

ABSTRACT: Bimetallic $Au_{75}Pd_{25}$ nanocrystals with shapes of icosahedron and octahedron were synthesized by adding different amounts of iodide ions, and were employed as catalysts for solvent-free aerobic oxidation of cyclohexane. Although both icosahedrons and octahedrons were bounded by {111} facets, the turnover frequency number of $Au_{75}Pd_{25}$ icosahedrons reached 15 106 h^{-1}, almost three times as high as that of $Au_{75}Pd_{25}$ octahedrons. The conversion of cyclohexane reached 28.1% after 48 h using $Au_{75}Pd_{25}$ icosahedrons, with the selectivity of 84.3% to cyclohexanone. Density functional theory calculations along with X-ray photoelectron spectroscopy examinations reveal that the excellent catalytic performance of AuPd icosahedrons could be ascribed to twin-induced strain and highly negative charge density of Au atoms on the surface.

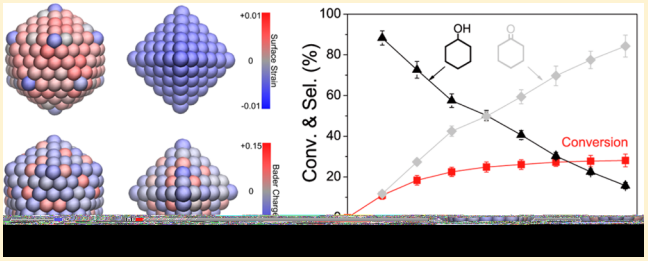

KEYWORDS: *aerobic oxidation, cyclohexane, DFT, gold, palladium, icosahedron*

The aerobic oxidation of cyclohexane is crucial in the chemical industry, because the products of this reaction, cyclohexanol and cyclohexanone, play pivotal roles as feedstock in a variety of reactions.[1,2] For example, serving as the precursors to nylon-6 and nylon-6,6, millions of tons of cyclohexanol and cyclohexanone are consumed every year.[1] It is generally accepted that for this reaction, molecular oxygen is among the most efficient, economical and environmentally friendly oxidants. However, considering the high stability of an O_2 molecule with a bond length of 121 pm and a bond energy of 498 kJ/mol, it takes much energy to break the double bond in the molecule. It still remains as a challenge to fabricate highly efficient catalysts to activate oxygen molecules. Another limitation is the difficulty in controlling the selectivity to the desired products. Au/ZSM5, graphene/g-C_3N_4, and FeAlPO have been applied as catalysts for the aerobic oxidation of cyclohexane, but both the activity and selectivity were limited (Supporting Information Table S1).[3] To date, the best catalytic performance was achieved by using Au_{39}/HAP, where the conversion reached 14.9% with selectivity for cyclohexanone of 49%.[4]

Heterogeneous catalysis of metal nanocrystals is dependent on multiple factors, including particle size,[5,6] exposed facet,[7−15] defective microstructure,[16−20] and elemental composition.[21−30] As a typical case of defective microstructures, twin defect, induced by a disruptive change of the long-range stacking sequence over substantial atomic spacing,[31] is especially determinant to the performance of catalysts. Even enclosed by the same crystal facets, nanocrystals with or without twin defects can exhibit distinctively different catalytic activities. Recent studies have been paid attention to the effects of twin defects on catalysis, discovering that twin defects usually endow metals with higher catalytic activity.[16−20,32−34] For example, as well-defined face-centered-cubic (*fcc*) nanocrystals, tetrahedrons, octahedrons, decahedrons, and icosahedrons are all enclosed by {111} facets. Tetrahedrons and octahedrons are single crystals, while decahedrons and icosahedrons are constructed with twin defects, the latter group clearly showing higher activity. However, the mechanism of this effect has not been fully elucidated to date. This work, based on the successful synthesis of highly effective catalysts for aerobic oxidation of cyclohexane, provides a detailed investigation of the influence of twinned structures in catalysis.

Herein, $Au_{75}Pd_{25}$ icosahedrons and octahedrons were successfully synthesized by adding different amounts of iodide ions and then were applied in the aerobic oxidation of cyclohexane. At a reaction time of 12 h, the conversion and TOF number of $Au_{75}Pd_{25}$ icosahedrons reached 18.4% and 15 106 h^{-1}, respectively, both of which were almost three times as high as those of the octahedrons. When the reaction proceeded to 48 h, the conversion of cyclohexane increased to 28%, while the selectivity for cyclohexanone was maintained as

Received: November 25, 2014
Revised: March 24, 2015
Published: April 3, 2015

DOI: 10.1021/nl5045132
Nano Lett. 2015, 15, 2875−2880

84.3%. Additionally, 85% of the initial catalytic activity was preserved after five rounds of the reaction, indicating a noticeable stability of $Au_{75}Pd_{25}$ icosahedrons. Density functional theory (DFT) calculations revealed that the high catalytic activity of the $Au_{75}Pd_{25}$ icosahedrons was associated with its tensile surface structure and highly negative charge density of surface Au atoms.

In a typical synthesis of $Au_{75}Pd_{25}$ icosahedrons, $HAuCl_4$ (20 mM, 0.75 mL), $Pd(acac)_2$ (2 mM, 2.5 mL), polyvinylpyrrolidone (PVP) (150 mg), and KI (10 mM, 0.05 mL) were mixed with 10 mL of *N*,*N*-dimethylformamide (DMF) in a 20 mL glass vial. After the vial had been capped, the mixture was ultrasonicated for about 2 min. The resulting homogeneous mixture was transferred into an oven and heated at 140 °C for 4 h. After cooling down to room temperature, the mixture was centrifugated for 15 min and washed four times with ethanol in order to collect the products. Figure 1a,b shows a transmission electron microscopy (TEM) image and a high-angle annular dark-field scanning TEM (HAADF-STEM) image of the AuPd nanocrystals, respectively, implying that the nanocrystal had an icosahedral shape with a narrow size distribution. From the TEM image, an average edge length of 7.5 nm was derived for the AuPd icosahedrons (Supporting Information Figure S1).

Figure 1. (a) TEM and (b) HAADF-STEM images of AuPd icosahedrons. (c) STEM image of an individual AuPd icosahedron. (d) Atomic-resolution STEM image taken from the edge of a single AuPd icosahedron, showing twin boundary. (e) STEM image and STEM-EDX elemental mapping images of an individual nanocrystal. Red corresponds to Au, where green corresponds to Pd. (f) Compositional line-scanning profile of the AuPd alloy icosahedron. The inset image in panel a is a schematic illustration of the icosahedral structure.

The inset in Figure 1a shows a schematic illustration of an individual icosahedral structure. The icosahedron, enclosed by 20 {111} facets, was made of 20 tetrahedral subunits with 30 twin boundaries. Figure1c,d shows STEM images of an individual AuPd icosahedron, through which twinned structures could be clearly observed. As shown by the STEM image and STEM-energy dispersive X-ray (STEM-EDX) elemental mapping of an individual AuPd icosahedron (Figure 1e), both Au and Pd were homogeneously distributed, indicating the formation of AuPd alloy. The compositional line-scanning profile of the icosahedron in Figure 1f indicates that it was indeed AuPd alloy without significant segregation for each component.

The procedure for the preparation of AuPd octahedrons is similar to what was used for AuPd icosahedrons except for the amount of KI (0.2 mL of 10 mM KI for octahedrons). As revealed by the TEM and HAADF-STEM images (Figure 2a,b),

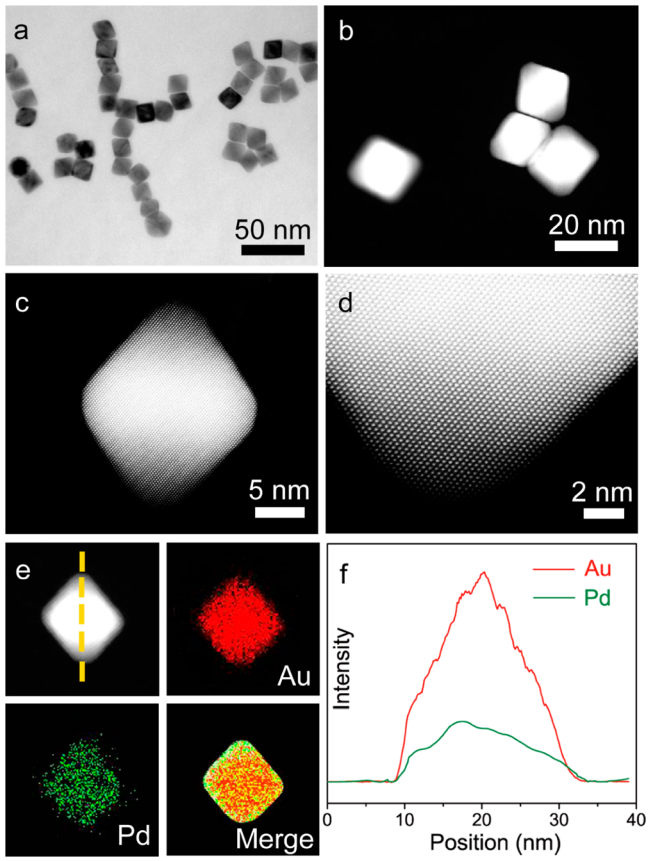

Figure 2. (a) TEM and (b) HAADF-STEM images of AuPd octahedrons. (c) STEM image of an individual AuPd octahedron. (d) Atomic-resolution STEM image taken from the edge of a single AuPd octahedron. (e) STEM image and STEM-EDX elemental mapping images of an individual nanocrystal. Red corresponds to Au while green corresponds to Pd. (f) Compositional line-scanning profile of the AuPd alloy octahedron.

the octahedrons were uniform in size, with an average edge length of about 15.4 nm (Supporting Information Figure S1). We also employed a series of tools to analyze the structures and characterize the chemical composition of AuPd octahedrons. The STEM images (Figure 2c,d) show an individual AuPd octahedron enclosed by {111} facets without twin defects. As shown by the STEM image and STEM-EDX elemental

DOI: 10.1021/nl5045132
Nano Lett. 2015, 15, 2875−2880

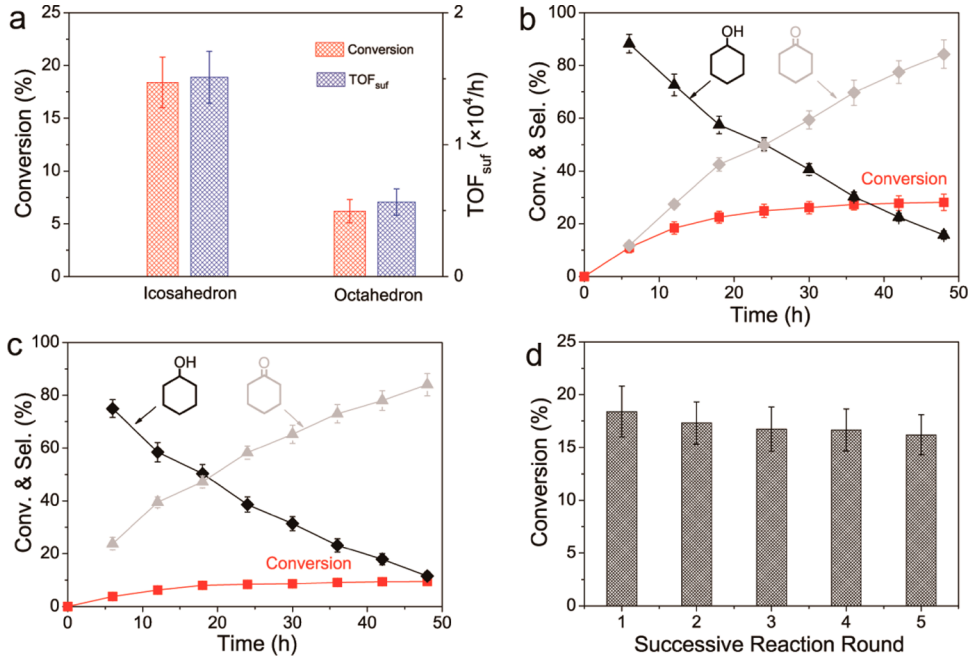

Figure 3. Comparison of the catalytic activity of $Au_{75}Pd_{25}$ alloy icosahedrons and octahedrons for cyclohexane oxidation. (a) Conversion and TOF for cyclohexane for $Au_{75}Pd_{25}$ alloy icosahedrons and octahedrons. Time course of the oxidation of cyclohexane with 10 atm O_2 catalyzed by $Au_{75}Pd_{25}$ (b) icosahedrons and (c) octahedrons at 125 °C, respectively. (d) Relative activity of $Au_{75}Pd_{25}$ icosahedrons over the course of five rounds of successive reaction.

mapping of an individual octahedron (Figure 2e), both Au and Pd were distributed evenly in the octahedron. The compositional line-scanning profile of the octahedron (Figure 2f) further indicates the formation of an alloyed AuPd octahedron. Despite the differences in morphology, the atomic contents of both products were determined to be $Au_{75}Pd_{25}$ by inductively coupled plasma atomic emission spectroscopy (ICP-AES), well consistent with the molar ratio of two precursors supplied. Nearly all of the metal precursors (>97%) were reduced within 2 h based on the ICP-AES data of Au and Pd remaining in the reaction solution (Supporting Information Figure S2).

It is known that oxidative etching has a crucial impact on the morphology of resultant nanocrystals. One function of oxidative etching is to selectively remove twinned seeds. The defects inherently existing in twinned seeds serve as active sites for oxidative dissolution, leading to preferential etching and dissolution of twinned seeds in an oxidative environment.[35] In addition, through removing new nuclei in the growth stage of nanocrystals, oxidative etching is expected to increase the size uniformity of the product.[35] In this work, we believed that the O_2/I^- pair was responsible for the oxidative etching. In the absence of KI, the product was dominated by AuPd icosahedrons with a broad size distribution (Supporting Information Figure S3a). When a small volume of KI (0.05 mL, 10 mM) was added, AuPd icosahedrons in high size uniformity were observed where the O_2/I^- pair effectively inhibited new nucleation in the growth stage. By comparison, more addition of KI (0.2 mL, 10 mM) would enhance the capability of oxidative etching, leading to selective etching away of twinned seeds. In this case, single-crystal AuPd octahedrons formed. Besides, when the synthesis was performed under nitrogen atmosphere instead of air, oxidative etching in this reaction was blocked, resulting in the formation of a product dominated by twinned nanocrystals in different shapes (Supporting Information Figure S3b).

The aerobic oxidation of cyclohexane was chosen as a sample reaction to evaluate the catalytic performance of the as-prepared AuPd icosahedrons and octahedrons. The blank test was performed with only active carbon added, during which no product was observed (Supporting Information Table S2, Entries 1 and 2). Parallel trials with temperature as a variable were conducted (Supporting Information Table S2, Entries 3 and 5–7). No reaction was observed at 75 °C. At 100 °C the reaction proceeded with a relatively low conversion. By contrast, the reaction was accelerated with the highest selectivity at 125 °C and a lower selectivity at 150 °C. The conversion showed an upward trend, whereas the selectivity exhibited a downward trend with the increase of temperature. To this end, at 125 °C—under which relatively high conversion and satisfactory selectivity were reached—was selected as the optimal temperature to conduct the following experiments. Figure 3a shows the catalytic performance of $Au_{75}Pd_{25}$ icosahedrons and octahedrons. Under the same reaction condition (125 °C, 12 h), the conversion reached 18.4% for the reaction involving icosahedrons, being 2.97 times as high as that of octahedrons. In addition, a TOF of 15 106 h^{-1} was observed for icosahedrons, which was 2.68 times as high as that of octahedrons. The reaction profile of product converting over time using $Au_{75}Pd_{25}$ icosahedrons is illustrated in Figure 3b. The conversion for cyclohexane was increased to almost 28.1% after 48 h of reaction, during which the products contained only cyclohexane and cyclohexanol without other byproducts. In addition, the content of cyclohexanone increased and that of cyclohexanol dropped, because more cyclohexanol was oxidized to cyclohexanone when the reaction proceeded. After 48 h of reaction, the percentage of cyclohexanone in the products reached 84.3%. By comparison, when $Au_{75}Pd_{25}$ octahedrons were utilized instead, the conversion only reached 9.5% after 48 h, with selectivity for cyclohexanone standing at 84.0% (Figure 3c). Carbon balance and ICP-AES analysis showed that most of

DOI: 10.1021/nl5045132
Nano Lett. 2015, 15, 2875–2880

the metals (>98%) were reserved for both AuPd icosahedrons and octahedrons after the reaction (Supporting Information Table S3). The stability of $Au_{75}Pd_{25}$ icosahedrons was also studied by performing successive rounds of reaction, as shown in Figure 3d. After five rounds, almost 85% of the original reaction activity was preserved, showing high stability of $Au_{75}Pd_{25}$ icosahedrons. TEM images (Supporting Information Figure S4) indicated that the morphology of $Au_{75}Pd_{25}$ icosahedrons was barely changed, whereas ICP-AES data and carbon balance implied that more than 95% of the noble metals were preserved in the reuse test (Supporting Information Table S3).

DFT calculations were performed to investigate the difference in activity between $Au_{75}Pd_{25}$ icosahedrons and octahedrons. The models of pure Au icosahedrons and octahedrons are shown in Supporting Information Figure S5, and the models of $Au_{75}Pd_{25}$ icosahedrons and octahedrons are shown in Supporting Information Figure S6. First-principles simulations were performed to calculate the strain fields on the surface of icosahedrons and octahedrons. For single-crystal nanocrystals, surface stress is the consequence of spontaneous bond contraction.[36] As shown in Supporting Information Figure S7 and Supporting Information Table S4, the surface strain on a pure Au icosahedron is tensile (averaging +0.51%), whereas that on a pure Au octahedron is compressive (average −3.26%). The difference in surface strain (3%−4%) is also observed for the cases of $Au_{75}Pd_{25}$ icosahedrons and octahedrons shown in Figure 4a,b. Surface strain influences the electronic structure of surface atoms through shifting their d-band center, which results in the variations of adsorption strength.[16,37] DFT calculations show a large difference in the d-band center (0.11 eV) between $Au_{75}Pd_{25}$ icosahedrons and octahedrons (Supporting Information Figure S8). Similar discrepancy was also observed for the cases of pure Au icosahedrons and octahedrons (Supporting Information Figure S9 and Table S5). A tensile strain can shift up d-band center and, thus, increase the adsorption strengths, which would help promote the adsorption of cyclohexane onto the catalyst.[37,38] To this end, the activation of C−H bonds in alkanes could be much facilitated.[37,38] These tendencies are consistent with our experimental results, in which the activity and strain changes on $Au_{75}Pd_{25}$ icosahedrons and octahedrons. Although nanocrystals used in the calculations are smaller than those in the experiments, conclusions could be still applied in the latter case because the trend of strain is preserved in the range of 1−20 nm.[36,39,40]

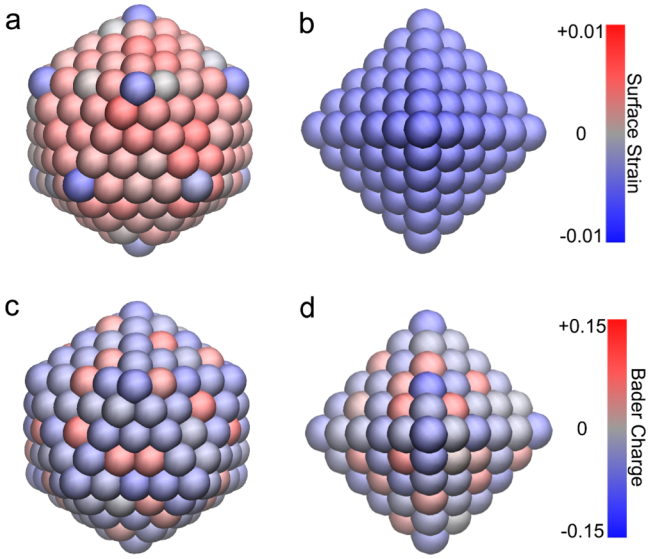

Figure 4. Surface strain of $Au_{75}Pd_{25}$ (a) icosahedrons and (b) octahedrons. Color indicates strain labeled in the color map, where a blue value means that there is compressive strain on the facets. Bader charge of $Au_{75}Pd_{25}$ (c) icosahedrons and (d) octahedrons. Color indicates Bader charge labeled in the color map, where a blue value means that the atom receives electrons.

In addition of the surface strain, the surface electronic property is also believed to be influential to catalytic activity. DFT simulations were conducted to calculate the charge transfer between atoms in $Au_{75}Pd_{25}$ alloy nanocrystals. The average charge per surface atom in pure Au icosahedrons and octahedrons were −0.027 e and −0.023 e, respectively (Supporting Information Figure S10 and Table S6). After introducing Pd atoms, the composition effect was obviously observed, and the negative charge densities increased to −0.060 e and −0.051 e per surface Au atom in $Au_{75}Pd_{25}$ icosahedron and octahedron, respectively (Figure 4c,d). Obviously, the surface negative charge for icosahedrons is denser than that of octahedrons for both pure Au and $Au_{75}Pd_{25}$ nanocrystals. These calculations reveal that the Pd atoms donate electrons to the Au atoms. To further confirm this electron donation, we examined the electronic properties of $Au_{75}Pd_{25}$ icosahedrons and octahedrons using X-ray photoelectron spectroscopy (XPS). As shown in Figure 5, the binding energy of Au $4f_{7/2}$ in the $Au_{75}Pd_{25}$ octahedrons equaled to that of bulk Au (84.0 eV), which suggests few electron transfers between Pd atoms and Au atoms. In contrast, the binding energies of Au 4f (including $4f_{7/2}$ and $4f_{5/2}$) and Au $3d_{5/2}$ in $Au_{75}Pd_{25}$ icosahedron were 0.8 and 0.6 eV lower compared with the case of $Au_{75}Pd_{25}$ octahedron, respectively. Meanwhile, the binding energy of Pd 3d (including $3d_{5/2}$ and $3d_{3/2}$) in $Au_{75}Pd_{25}$ icosahedrons was 0.4 eV higher than that of $Au_{75}Pd_{25}$ octahedrons. The negative shift of Au 4f and the positive shift of Pd 3d suggest that a negative charge was deposited on the Au atoms of $Au_{75}Pd_{25}$ icosahedrons, which is consistent with calculated results. Considering that hydroperoxo-like molecular oxygen species, an important intermediate in the aerobic oxidation reaction, was favorably generated on negative charged surface, anionic charges on surface Au atoms contributed largely to the catalytic performance in the aerobic oxidation reactions.[25,41] Taking surface strain and surface charge transfer into account, we can conclude that the high catalytic activity of $Au_{75}Pd_{25}$ icosahedrons was attributed to the tensile surface structure and highly negative charge density of surface Au atoms.

In conclusion, we synthesized $Au_{75}Pd_{25}$ icosahedrons and octahedrons, and utilized them as the catalysts for the aerobic oxidation of cyclohexane. Although both icosahedrons and octahedrons were bounded by {111} facets, the TOF of $Au_{75}Pd_{25}$ icosahedrons was almost three times as high as that of $Au_{75}Pd_{25}$ octahedrons, reaching the value of 15 106 h^{-1}. Moreover, the conversion of cyclohexane reached 28.1% after 48 h using $Au_{75}Pd_{25}$ icosahedrons as the catalyst, with selectivity for cyclohexanone of 84.3%. Further theoretical analysis confirms that twins in $Au_{75}Pd_{25}$ icosahedrons predominately generated tensile surface structure and highly negative charge density surface, which could enhance the catalytic activity. This research concerning twinned structure is anticipated to raise widespread interests about potential use of twins in more aerobic oxidation reactions.

DOI: 10.1021/nl5045132
Nano Lett. 2015, 15, 2875−2880

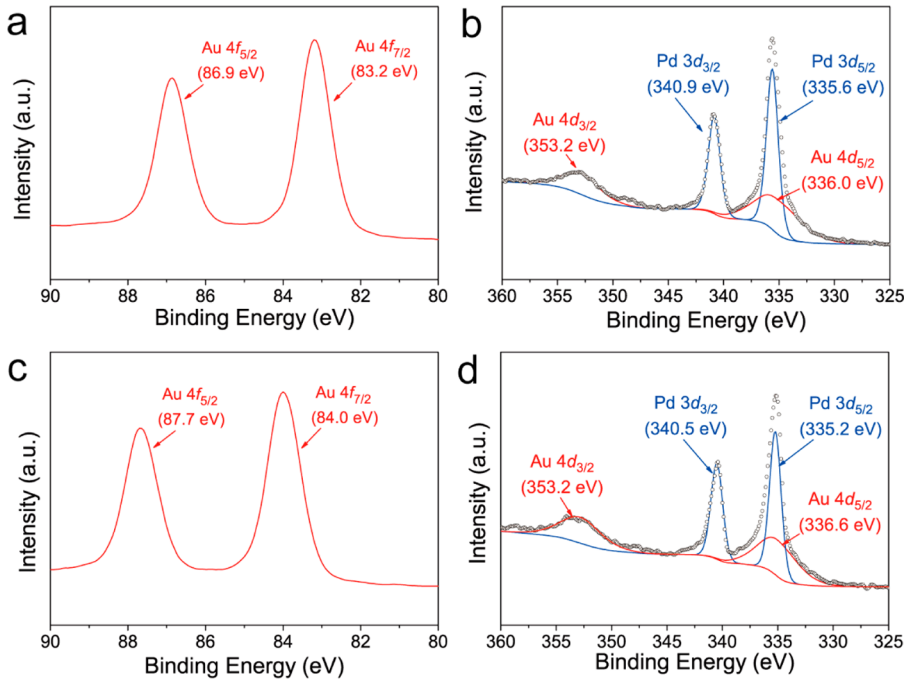

Figure 5. XPS spectra of $Au_{75}Pd_{25}$ (a, b) icosahedron and (c, d) octahedron.

■ ASSOCIATED CONTENT

Supporting Information

Experimental details, catalytic performance in the aerobic oxidation of cyclohexane that was reported previously, histograms of particle size distribution, percentages of Au and Pd species remaining in the reaction solution, TEM image of the products, the aerobic oxidation of cyclohexane catalyzed by $Au_{75}Pd_{25}$ icosahedrons and octahedrons, carbon balance and residual metal of AuPd icosahedrons and octahedrons after different rounds of the reaction, TEM images of $Au_{75}Pd_{25}$ icosahedrons, atomic structures of (a) a Au icosahedron with 309 atoms and (b) a Au octahedron with 146 atoms, atomic structures of (a) a $Au_{75}Pd_{25}$ icosahedron with 309 atoms and (b) a $Au_{75}Pd_{25}$ octahedron with 146 atoms, surface strain on (a) a Au icosahedron and (b) a Au octahedron, surface strain fields on Au and $Au_{75}Pd_{25}$ nanocrystals, projected d-DOS of surface atoms on $Au_{75}Pd_{25}$ nanocrystals, projected d-DOS of surface atoms on Au nanocrystals, the d-band center of surface atoms on Au and $Au_{75}Pd_{25}$ nanocrystals, Bader charges on (a) a Au icosahedron and (b) a Au octahedron, Bader charges of surface Au atoms on Au and $Au_{75}Pd_{25}$ nanocrystals, additional references. This material is available free of charge via the Internet at http://pubs.acs.org.

■ AUTHOR INFORMATION

Corresponding Authors

*E-mail: zengj@ustc.edu.cn.
*E-mail: zyli@ustc.edu.cn.

Author Contributions

†These authors contributed equally.

Notes

The authors declare no competing financial interest.

■ ACKNOWLEDGMENTS

This work was supported by Collaborative Innovation Center of Suzhou Nano Science and Technology, MOST of China (2014CB932700 and 2011CB921403), SRG-HSC, NSFC under Grant Nos. 21203173, 21222304, 51371164, 21121003, 51132007 and J1030412, Strategic Priority Research Program B of the CAS under Grant No. XDB01020000, and Fundamental Research Funds for the Central Universities (WK2340000050 and WK2060190025).

■ REFERENCES

(1) Jevtic, R. *The Effect of Oxygen on the Oxidation of Cyclohexane*; Proquest: Ann Arbor, MI, 2011).

(2) Clerici, M. G. *Liquid Phase Oxidation via Heterogeneous Catalysis: Organic Synthesis and Industrial Applications*; Wiley: Hoboken, NJ, 2013.

(3) The references concerning aerobic oxidation of cyclohexane are listed in Supporting Information Table S1.

(4) Liu, Y.; Tsunoyama, H.; Akita, T.; Xie, S.; Tsukuda, T. *ACS Catal.* **2011**, *1*, 2−6.

(5) Corma, A.; Concepcion, P.; Boronat, M.; Sabater, M. J.; Navas, J.; Yacaman, M. J.; Larios, E.; Posadas, A.; Lopez-Quintela, M. A.; Buceta, D.; Mendoza, E.; Guilera, G.; Mayoral, A. *Nat. Chem.* **2013**, *5*, 775−781.

(6) Song, H.; Rioux, R. M.; Hoefelmeyer, J. D.; Komor, R.; Niesz, K.; Grass, M.; Yang, P.; Somorjai, G. A. *J. Am. Chem. Soc.* **2006**, *128*, 3027−3037.

(7) Tian, N.; Zhou, Z. Y.; Sun, S.; Ding, Y.; Wang, Z. L. *Science* **2007**, *316*, 732−735.

(8) Lee, I.; Delbecq, F.; Morales, R.; Albiter, M. A.; Zaera, F. *Nat. Mater.* **2009**, *8*, 132−138.

(9) Kang, Y.; Li, M.; Cai, Y.; Cargnello, M.; Diaz, R. E.; Gordon, T. R.; Wieder, N. L.; Adzic, R. R.; Gorte, R. J.; Stach, E. A.; Murray, C. B. *J. Am. Chem. Soc.* **2013**, *135*, 2741−2747.

(10) Collins, G.; Schmidt, M.; Dwyer, C. O.; Holmes, J. D.; McGlacken, G. P. *Angew. Chem., Int. Ed.* **2014**, *53*, 4142−4145.

(11) Yang, C. W.; Chanda, K.; Lin, P. H.; Wang, Y. N.; Liao, C. W.; Huang, M. H. *J. Am. Chem. Soc.* **2011**, *133*, 19993−20000.

(12) DeSantis, C. J.; Skrabalak, S. E. *J. Am. Chem. Soc.* **2013**, *135*, 10−13.

(13) Bower, M. M.; DeSantis, C. J.; Skrabalak, S. E. *J. Phys. Chem. C* **2014**, *118*, 18762−18770.

(14) Niu, W.; Zhang, L.; Xu, G. *ACS Nano* **2010**, *4*, 1987−1996.

DOI: 10.1021/nl5045132
Nano Lett. 2015, 15, 2875−2880

(15) Brodsky, C. N.; Young, A. P.; Ng, K. C.; Kuo, C. H.; Tsung, C. K. *ACS Nano* **2014**, *8*, 9368−9378.
(16) Wu, J.; Qi, L.; You, H. J.; Gross, A.; Li, J.; Yang, H. *J. Am. Chem. Soc.* **2012**, *134*, 11880−11883.
(17) Walsh, M. J.; Yoshida, K.; Kuwabara, A.; Pay, M. L.; Gai, P. L.; Boyes, E. D. *Nano Lett.* **2012**, *12*, 2027−2031.
(18) Yoon, J.; Khi, N. T.; Kim, H.; Kim, B.; Baik, H.; Back, S.; Lee, S.; Lee, S. W.; Kwon, S. J.; Lee, K. *Chem. Commun.* **2013**, *49*, 573−575.
(19) Bhattarai, N.; Casillas, G.; Ponce, A.; Jose-Yacaman, M. *Surf. Sci.* **2013**, *609*, 161−166.
(20) Lv, T.; Wang, Y.; Choi, S. I.; Chi, M.; Tao, J.; Pan, L.; Huang, C.; Zhu, Y.; Xia, Y. *ChemSusChem* **2013**, *6*, 1923−1930.
(21) Zhao, X.; Chen, S.; Fang, Z.; Ding, J.; Sang, W.; Wang, Y.; Zhao, J.; Peng, Z.; Zeng, J. *J. Am. Chem. Soc.* **2015**, *137*, 2804−2807.
(22) Enache, D. I.; Edwards, J. K.; Landon, P.; Solsona-Espriu, B.; Carley, A. F.; Herzing, A. A.; Watanabe, M.; Kiely, C. J.; Knight, D. W.; Hutchings, G. J. *Science* **2006**, *311*, 362−365.
(23) Sang, W.; Zheng, T.; Wang, Y.; Li, X.; Zhao, X.; Zeng, J.; Hou, J. G. *Nano Lett.* **2014**, *14*, 6666−6671.
(24) Wang, G. H.; Hilgert, J.; Richter, F. H.; Wang, F.; Bongard, H. J.; Spliethoff, B.; Weidenthaler, C.; Schuth, F. *Nat. Mater.* **2014**, *13*, 294−301.
(25) Zhang, H.; Watanabe, T.; Okumura, M.; Haruta, M.; Toshima, N. *Nat. Mater.* **2012**, *11*, 49−52.
(26) Chen, S.; Su, H.; Wang, Y.; Wu, W.; Zeng, J. *Angew. Chem., Int. Ed.* **2015**, *54*, 108−113.
(27) Hernandez-Fernandez, P.; Masini, F.; McCarthy, D. N.; Strebel, C. E.; Friebel, D.; Deiana, D.; Malacrida, P.; Nierhoff, A.; Bodin, A.; Wise, A. M.; Nielsen, J. H.; Hansen, T. W.; Nilsson, A.; Stephens, I. E. L.; Chorkendorff, I. *Nat. Chem.* **2014**, *6*, 732−738.
(28) Wang, L.; Yamauchi, Y. *J. Am. Chem. Soc.* **2013**, *135*, 16762−16765.
(29) Yu, W. Y.; Mullen, G. M.; Flaherty, D. W.; Mullins, C. B. *J. Am. Chem. Soc.* **2014**, *136*, 11070−11078.
(30) Kusada, K.; Kobayashi, H.; Ikeda, R.; Kubota, Y.; Takata, M.; Toh, S.; Yamamoto, T.; Matsumura, S.; Sumi, N.; Sato, K.; Nagaoka, K.; Kitagawa, H. *J. Am. Chem. Soc.* **2014**, *136*, 1864−1871.
(31) Xia, Y.; Xiong, Y.; Lim, B.; Skrabalak, S. E. *Angew. Chem., Int. Ed.* **2009**, *48*, 60−103.
(32) Kuo, C. H.; Lamontagne, L. K.; Brodsky, C. N.; Chou, L. Y.; Zhuang, J.; Sneed, B. T.; Sheehan, M. K.; Tsung, C. K. *ChemSusChem* **2013**, *6*, 1993−2000.
(33) He, R.; Wang, Y. C.; Wang, X.; Wang, Z.; Liu, G.; Zhou, W.; Wen, L.; Li, Q.; Wang, X.; Chen, X.; Zeng, J.; Hou, J. G. *Nat. Commun.* **2014**, *5*, 4327.
(34) Sneed, B. T.; Brodsky, C. N.; Kuo, C. H.; Lamontagne, L. K.; Jiang, Y.; Wang, Y.; Tao, F.; Huang, W.; Tsung, C. K. *J. Am. Chem. Soc.* **2013**, *135*, 14691−14700.
(35) Zheng, Y.; Zeng, J.; Ruditskiy, A.; Liu, M.; Xia, Y. *Chem. Mater.* **2014**, *26*, 23−33.
(36) Ouyang, G.; Li, X. L.; Tan, X.; Yang, G. W. *Appl. Phys. Lett.* **2006**, *89*, 031904.
(37) Hammer, B.; Norskov, J. K. *Adv. Catal.* **2000**, *45*, 71−129.
(38) Labinger, J. A.; Bercaw, J. E. *Nature* **2002**, *417*, 507−514.
(39) Qin, W.; Chen, Z. H.; Huang, P. Y.; Zhuang, Y. H. *J. Alloys Compd.* **1999**, *292*, 230−232.
(40) Nanda, K. K.; Behera, S. N.; Sahu, S. N. *J. Phys.: Condens. Matter* **2001**, *13*, 2861−2864.
(41) Woodham, A. P.; Meijer, G.; Fielicke, A. *Angew. Chem., Int. Ed.* **2012**, *51*, 4444−4447.

DOI: 10.1021/nl5045132
Nano Lett. 2015, 15, 2875−2880